ELSEVIER

Materials Science and Engineering A214 (1996) 133–138

MATERIALS SCIENCE & ENGINEERING A

Effect of magnesium on mechanical properties of Al_2O_3/ Al–Zn–Mg–Cu metal matrix composites formed by squeeze casting

Jer-Horng Hsieh, Chuen-Guang Chao

Institute of Materials Science and Engineering, National Chiao Tung University, Hsinchu, Taiwan

Abstract

Al_2O_3/Al–Zn–Mg–Cu composites containing 2.0 ~ 3.0 wt.% Mg in the matrix alloy have been fabricated by squeeze casting. Light microscopy, scanning electron microscopy and image analysis were used to examine and analyze the details of microstructure and the fracture surface. Tensile tests were utilized to evaluate the mechanical properties. The aging behavior of the composites was studied by using differential scanning calorimetry technique and microhardness tests. The microhardness and ultimate tensile strength (UTS) of the composites increase with increasing Mg content. The maximum microhardness and UTS of the composites occur at 120 °C aging for 24 h.

Keywords: Magnesium; Mechanical properties; Squeeze casting

1. Introduction

In the last decade, a substantial amount of work has been carried out on metal matrix composites. These materials usually combine the high Young's modulus and strength of a ceramic with the ductility of a metal. Most of the alloys that are employed as matrices in metal matrix composites (MMCs) are light alloys, particularly those based on aluminum such as 356 [1], 2xxx[2–5] and 6xxx [6–8] series. However, few studies have reported on the Al–Zn–Mg–Cu 7xxx series alloys which show the highest strength of all commercial aluminum alloys and are widely used for structural materials in military and civil aircraft. The aging behavior for Al–Zn–Mg–Cu alloys is generally recognized to take place in the following sequence [9–15]:

$$\text{supersaturated solid solution} \rightarrow \text{GP zones} \rightarrow \eta'(MgZn_2) \rightarrow \eta(MgZn_2)$$

The GP zones are coherent with the matrix; the interfacial energy is low so that small metastable particles can form. The semicoherent intermediate $MgZn_2$ phase, η', has been described as having a monoclinic unit cell while the incoherent equilibrium $MgZn_2$ phase, η, is hexagonal.

It is recognized that aluminum matrix composites may overage if given the same aging treatment as their unreinforced parent alloy [16]. Nieh and Karlar [17] found an accelerated aging effect owing to B_4C reinforcements in a 6061 aluminum alloy matrix. They suggested that the accelerated aging is primarily owing to the high dislocation density generated from thermal mismatch between the B_4C reinforcements and the aluminum matrix, and the presence of high diffusive interfaces in the composites. However, Stephens et al. [18] found no accelerated aging effect with large particles, which is consistent with the theory that the increase in dislocation density is inversely proportional to particle size. Dutta et al. [19] reported that the aging kinetics in cast materials is considerably slower than that in powder metallurgy processed materials. In addition, Bardhan and Starke Jr. [20] reported that magnesium plays the role of a reversible vacancy trap in Al–Zn–Mg alloys. High magnesium content induces a greater extent of quench clustering, resulting in a large as-quenched hardness difference in alloys with only slightly different magnesium contents. Our recent study [21] also showed that higher magnesium content induces a larger amount of GP zones and η' phase formation, resulting in increased microhardness of Al_2O_3/Al–Zn–Mg–Cu composites. In the present

work, magnesium was varied from 2.0 to 3.0 wt.% as an aid to increased age hardening of MMCs (Al_2O_3/ Al–Zn–Mg–Cu) produced by squeeze casting. The aging behavior of composites was studied by using differential scanning calorimetry (DSC) technique and hardness tests. We also studied the effect of magnesium on the mechanical properties of MMCs.

2. Experimental procedure

The composite materials were produced by squeeze casting. The aluminum matrix alloys were prepared to contain 2.0, 2.4 and 3.0 wt.% Mg, respectively, by melting 7075 Al and an Al-10 wt.% Mg master alloy. The composition of the Al-10 wt.% Mg alloy is 10.06 wt.% Mg, 0.01 wt.% Fe and 0.03 wt.% Si. The chemical compositions of the matrix alloys analyzed by inductively coupled plasma-mass spectrometer (ICP-MS) are listed in Table 1.

The basis of the fabrication technique has been described in our previous study [3]. The fiber volume fraction (V_f) of each composite was 0.1. The preform was preheated at 800 °C and introduced in the mold which was preheated to 300 °C. The liquid aluminum alloy at 800 °C was squeezed into fiber preform by a 40 Mpa hydraulic press to form the composites.

Microstructural characteristization was carried out by using light microscopy and scanning electron microscopy (SEM). Specimens were cut out from the casting as a cylindrical block 5.5 mm in diameter. Specimens were solution treated at 480 °C for 48 h, then quenched into water. Aging was carried out in an oil bath at 120 °C for various lengths of times from 4 to 96 h. All of the treated specimens were immediately stored in a refrigerator at −15 °C. Discs (5.5 mm diameter, 1 mm thickness) for DSC were polished and weighed. DSC analysis was performed by using a Dupont 2910 thermal analyzer. Disc samples were loaded in the DSC cell at room temperature and equilibrated for a few minutes. The heating rate was 10 °C min^{-1} from 50 to 450 °C. Dry nitrogen was purged through the cell at the rate of 40 ml min^{-1} to avoid oxidation. Output for all DSC runs was recorded in the instrumental memory. At least three samples were measured for each heat treatment. In order to evaluate the peak area of the DSC curve, the DSC scan of a sample was interrupted just as the η' formation reaction was finishing, and the DSC scan of the sample was run again as a baseline. A Vickers microhardness measurement on the matrix (between fibers) of heat-treated specimens was made using a diamond pyramid indenter and 50 g load. At least ten hardness measurements were made for each aging condition to ensure accurate results. Tensile specimens were machined to a gauge length of 13 mm with a cross-section of 2 mm × 4 mm. The tensile tests were carried out with an Instron machine with a 3×10^{-4} s^{-1}. The fracture surfaces were examined by SEM.

Table 1
Composition of the matrix alloys

Heat No.	Mg (wt.%)	Zn (wt.%)	Cu (wt.%)	Al (wt.%)
Heat 1	3.02	5.47	1.49	Bal
Heat 2	2.39	5.54	1.49	Bal
Heat 3	2.00	5.46	1.48	Bal

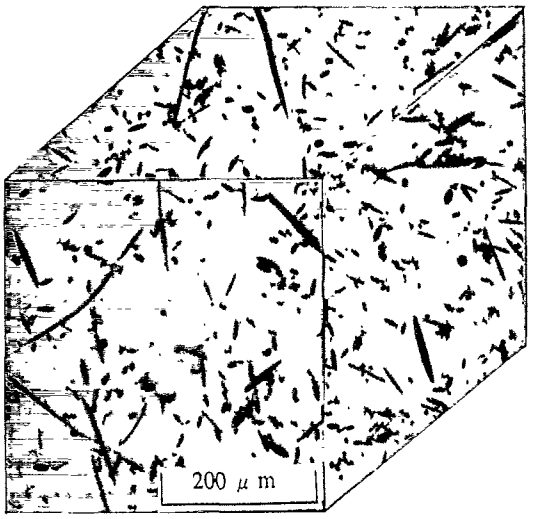

Fig. 1. 3-D light micrograph of the composite.

3. Results

3.1. Microstructure

Fig. 1 shows a 3-D light micrograph of the composite. The fibers were randomly distributed in the composite. Fig. 2 shows an etched light micrograph of "heat 3" in the Table 1 in the as-cast condition (a) the monolithic alloy and (b) the composite. Both materials have segregation in dendrite interstices. The dendrite arm spacing of the composite (about 12 μm) is smaller than that of the monolithic alloy (about 20 μm). It is suggested that Al_2O_3 fibers acted as obstacles during solidification.

3.2. DSC

3.2.1. Solution treatment

For comparison purposes, results from DSC scans of composites with 2.0 ~ 3.0 wt.% Mg quenched into water are shown in Fig. 3. The curve from the composite shows three regions: an exotherm between 75 °C and 140 °C owing to the dissolution of GP zones and precipitation of η' precursors (region 1); three exotherms

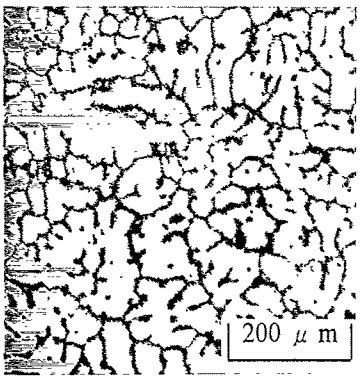

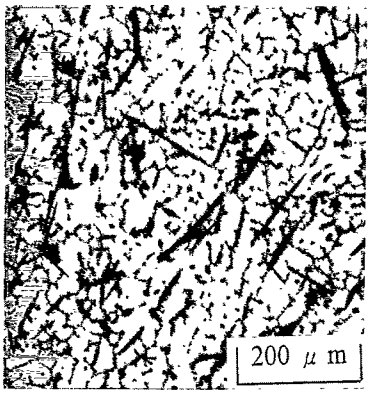

Fig. 2. Etched light micrographs of the as-cast materials (a) Al–Zn–Mg–Cu alloy (2.0 wt.% Mg) (b) 0.1 V_f composite.

between 140 °C and 300 °C (region 2) owing to the η' phase formation (peak A), the superimposed reactions of η' dissolution and η formation (peak B) and η precipitate growth (peak C); and an endotherm between 300 °C and 450 °C owing to the dissolution of η precipitate (region 3). The result is similar to the previous DSC work in 7xxx Al alloys [14,15].

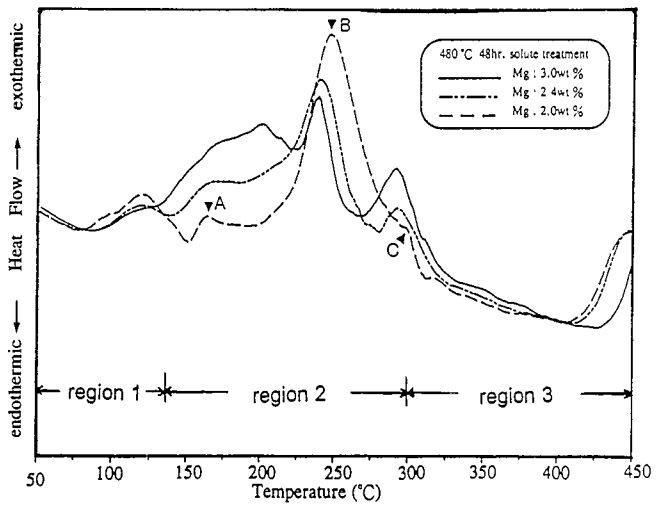

Fig. 3. Results of the DSC for solution treated composites with various Mg contents.

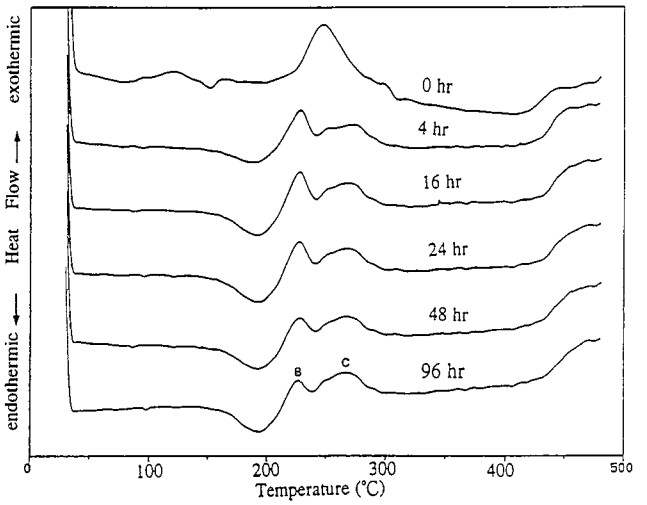

Fig. 4. Results of the DSC for solution treated composite (2.0 wt.% Mg) artificially aged at 120 °C for various aging times. Peak B: η' phase dissolution + η phase formation peak C: η phase growth.

3.2.2. Isothermal artificial aging

The results (Fig. 4) of DSC measurements on the composite (2.0 wt.% Mg) quenched from 480 °C into water and artificial aged at 120 °C for various aging periods (4, 16, 24, 48 and 96 h) indicate that peak B becomes progressively less and peak C becomes progressively more prominent with increasing in aging time. A similar trend was found in Figs. 5 and 6 for both 2.4 and 3.0 wt.% Mg composites, respectively.

3.3. Mechanical properties

3.3.1. Tensile properties

The Ultimate Tensile Strength (UTS) responses of the composites with 2.0 ~ 3.0 wt.% Mg as a function of aging time are shown in Fig. 7. All of the composites have the maximum value of UTS at aging for 24 h. The UTS of the composites increases with increasing Mg

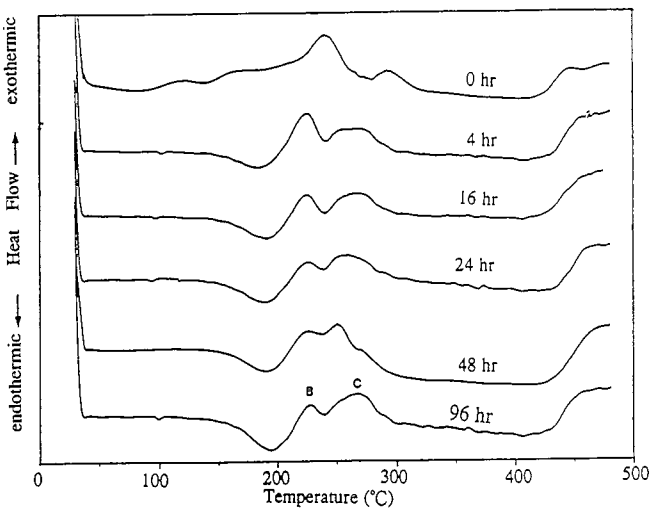

Fig. 5. Results of the DSC for a solution treated composite (2.4 wt% Mg) artificially aged at 120 °C for various aging times.

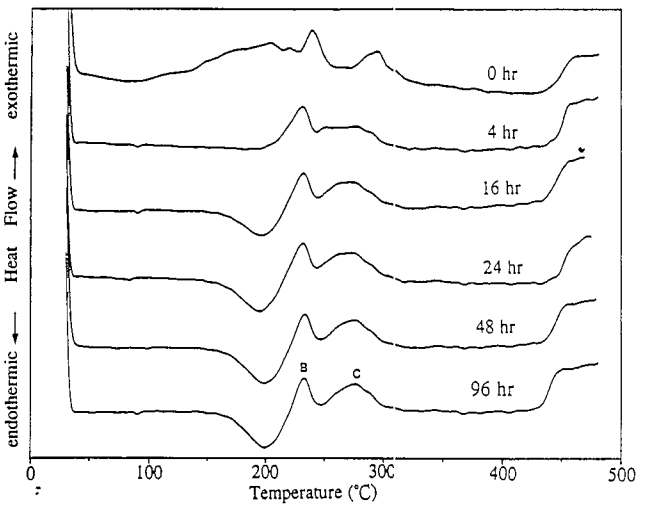

Fig. 6. Results of the DSC for a solution treated composite (3.0 wt.% Mg) artificially aged at 120 °C for various aging times.

content. Fig. 8 shows the elongation vs. aging time. The elongation of the composites is about 1 ~ 2%. However, that of the samples with solution treatment is about 3 ~ 5%.

3.4. Matrix microhardness

Fig. 9 shows the relationship between microhardness and aging time of the composites with various Mg content. It is assumed that the age-hardening treatment affects only the matrix properties. According to this investigation, the microhardness of the matrix in the composites displays the effect of Mg content on the aging characteristics of composite. The microhardness of the matrix at peak hardness (aged at 120 °C 24 h) increases with increasing Mg content.

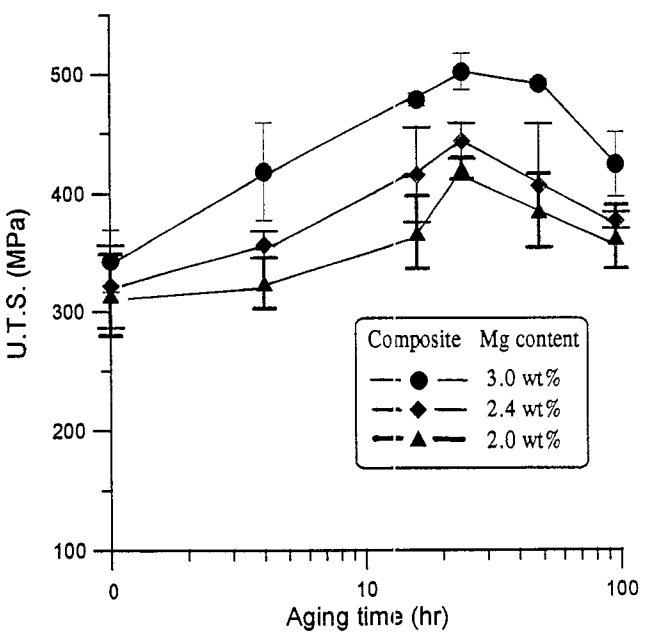

Fig. 7. Relationship between UTS and aging time of composites with various Mg contents.

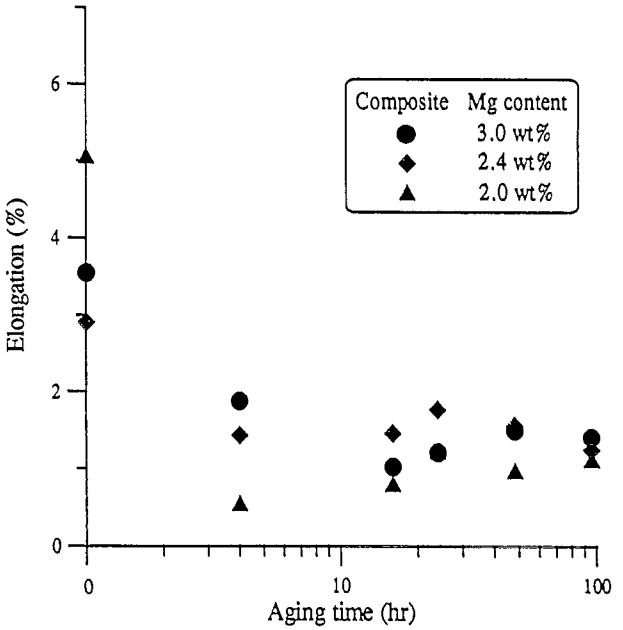

Fig. 8. Relationship between elongation and aging time of composites with various Mg contents.

4. Discussion

The curves in Fig. 3 show that the enthalpy of η' phase formation (peak A) is significantly different. The difference of these curves is owing to superimposed phenomena. Fig. 10 shows a schematic model to explain this difference. The basic assumptions are as follows:

(1) Only η' phase formation, η' phase dissolution, η phase formation and η phase growth occur in region 2.

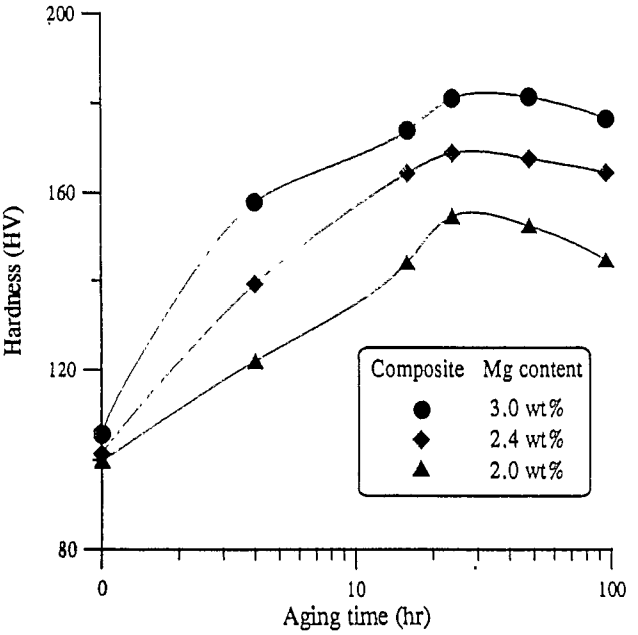

Fig. 9. Relationship between microhardness and aging time of composites with various contents.

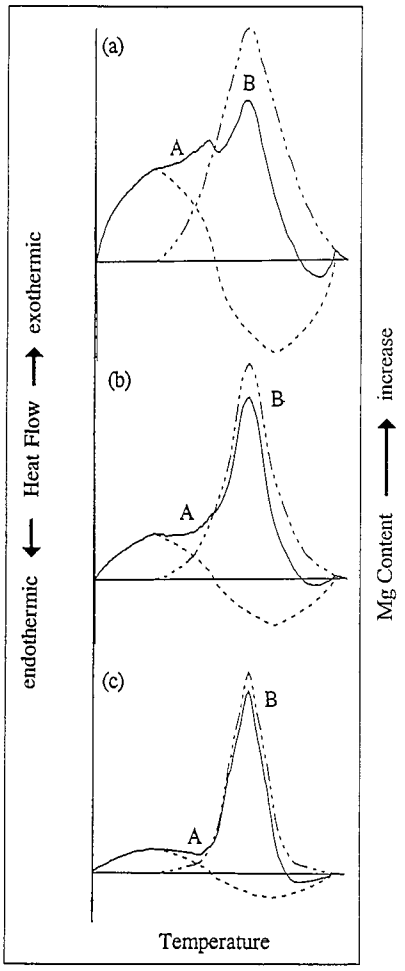

Fig. 10. Schematic model of DSC curve superimposed condition.

(2) The Mg solute atom in Al, which has a strong binding force with vacancies, may assist the precipitate process [12]. The amount of η' phase increases with increasing Mg content.
(3) The area of the η' phase formation peak in the DSC curve is equal to that of the η' phase dissolution peak.

The dotted line in Fig. 10 represents the peaks before the superimposed condition. The solid line is the final curve after the superimposed condition. Fig. 10 shows that peak A shifts to higher temperature but peak B shifts to lower temperature with increasing Mg content. It also shows that the peak value of peak A is increased and the peak value of peak B is decreased with increasing Mg content. The result is very close to that shown in Fig. 3. This indicates that the amount of η' phase formation increases with increasing Mg content. Fig. 4 ~ 6 show the results of DSC measurements on composites with 2.0 ~ 3.0 wt.% Mg content for various aging periods. The η' phase formation peak (peak A) disappears after artificial aging for 4 h, and an endotherm peak occurs between 140 °C and 220 °C, which is the η' phase dissolution peak. During the same time, the value of peak B (η' phase dissolution + η phase formation) progressively decreases and that of peak C (η phase growth) progressively increases.

When the aging time is more than 24 h, the value of peak C is larger than that of peak B, i.e. the amount of η phase growth is larger than that of η phase formation. This indicates that the composites are overaging beyond an aging time of 24 h. These results also match Figs. 7 and 9. The maximum microhardness (Mg 3.0 wt.%, Hv = 181; Mg 2.4 wt.%, Hv = 169; Mg 2.0 wt.%, Hv = 154) and UTS (Mg 3.0 wt.%, 520 Mpa; Mg 2.4 wt.%, 468 MPa; Mg 2.0 wt.%, 429 MPa) of the composites occurred at 120 °C aging for 24 h. Fig. 11 shows an SEM image of the broken fiber area of the composite. The fracture surface of the composite shows broken fibers within the dimple. This observation indicates that the bonding between the matrix and the fibers is good. However, microshrinkage porosity is observed in an SEM fractograph of the composites (see Fig. 12). Since the applied pressure (40 Mpa) is not high enough to eliminate the microshrinkage, the elongation of the composites is less than 2%.

5. Conclusion

In our present study, the Mg content from 2.0 to 3.0 wt.% affects the mechanical properties of Al_2O_3/Al–Zn–Mg–Cu composites. The results are summarized as follows:

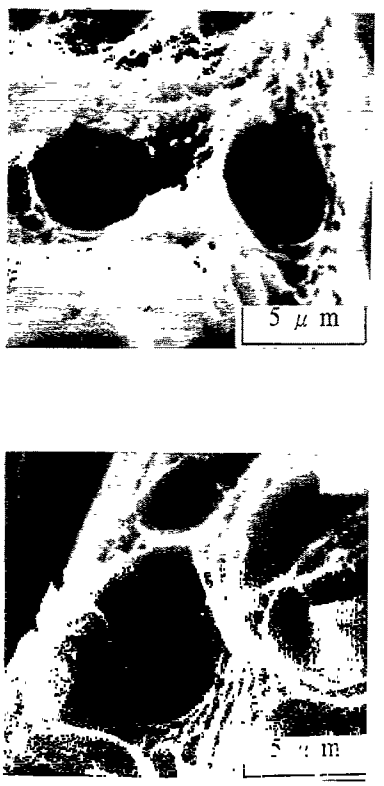

Fig. 11. SEM image of the broken fiber area of the composite (3.0% Mg) (a) solution treatment (b) aged 96 h.

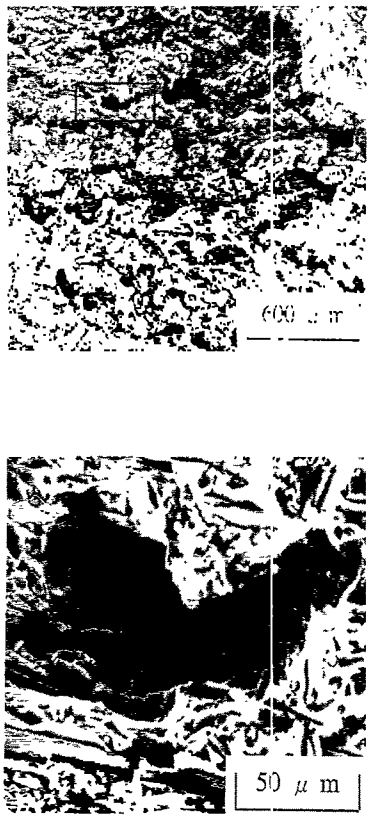

Fig. 12. (a) SEM fractography of the composite (b) enlarge area of microshrinkage.

(1) The microhardness and UTS of the composites increases with increasing Mg content.
(2) The maximum UTS of the composites occurred at 120 °C aging for 24 h. (Mg 3.0 wt.%, 520 Mpa; Mg 2.4 wt.%, 468 MPa; Mg 2.0 wt.%, 429 MPa)
(3) The maximum microhardness of the composites occurred at 120 °C aging for 24 h. (Mg 3.0 wt.%, Hv = 181; Mg 2.4 wt.%, Hv = 169; Mg 2.0 wt.%, Hv = 154)The elongation of the composites is about 3% ~ 5% after solution treatment and is about 1% ~ 2% after aging treatment.

Acknowledgements

The authors are pleased to acknowledge financial support of this research by National Science Council, Taiwan, under Grant NSC 82-0405-E-009-410.

References

[1] L. Wei and J.C. Huang, *Mater. Sci. Technol.*, *9* (1993) 841–852.
[2] P.G. Karandikar and T.W. Chou, *J. Mater. Sci.*, *26* (1991) 2573–2578.
[3] K.C. Chen and C.G. Chao, *Met. Mater. Trans. A*, *26A* (1995) 1035–1043.
[4] T. Christman and S. Suresh, *Acta Metall.*, *36* (7) (1988) 1691–1704.
[5] H. Jeong, D.K. Hsu, R.E. Shannon and P.K. Liaw, *Met. Mater. Trans. A*, *25A* (1994) 799–809.
[6] C.C. Perng, J.R. Hwang and J.L. Doong, *Mater. Sci. Eng.*, *A171* (1993) 213–221.
[7] D.J. Towle and C.M. Friend, *J. Mater. Sci.*, *27* (1992) 2781–2791.
[8] L. Salvo and M. Suery, *Mater. Sci. Eng.*, *A177* (1994) 19–28.
[9] N.C. Danh, K. Rajan and W. Wallace, *Metall. Trans. A*, *14A* (1983) 1843–1850.
[10] P. Bardhan and E.A. Starke Jr., *J. Mater. Sci.*, *3* (1968) 577–583.
[11] P.N. Adler and R. DeIasi, *Metall. Trans. A*, *8A* (1977) 1185–1190.
[12] J.D. Embury and R.B. Nicholson, *Acta Metall.*, *13* (1965) 403–417.
[13] E. Donoso, *Mater. Sci. Eng.*, *74* (1985) 39–46.
[14] D.J. Lloyd and M. C. Chaturvedi, *J. Mater. Sci.*, (1982) 1819–1824.
[15] J.L. Petty-Galis and R.D. Goolsby, *J. Mater. Sci.*, *24* (1989) 1439–1446.
[16] M. Vogelsang, R.J. Arsenault and R.M. Fisher, *Metall. Trans. A*, *17A* (1986) 379–389.
[17] T.G. Nieh and R.F. Karlak, *Scr. Metall.*, *18* (1984) 25–28.
[18] J.J. Stephens, J.P. Lucas and F.M. Hosking, *Scr. Metall.*, *22* (1988) 1307–1312.
[19] I. Dutta and D.L. Bourell, *Mater. Sci. Eng.*, *A112* (1989) 67.
[20] G. Honyek, I. Kovacs, J. Lendai, Ng-huy-sinh, T. Ungar, H. Loffler and R. Gerlach, *J. Mater. Sci.*, *16* (1981) 2701–2709.
[21] M.C. Chou and C.G. Chao, *Met. Mater. Trans. A.*, accepted for publication.